Appl. Magn. Reson. 31, 271–299 (2007)

Applied Magnetic Resonance

EPR Measurements of Weak Exchange Interactions Coupling Unpaired Spins in Model Compounds

R. Calvo

Departamento de Física, Facultad de Bioquímica y Ciencias Biológicas and
Instituto de Desarollo Tecnológico para la Industria Quimica,
Consejo Nacional de Investigaciones Científicas y Técnicas,
Universidad Nacional del Litoral, Santa Fe, Argentina

Received August 6, 2006; revised September 8, 2006

Abstract. I review electron paramagnetic resonance (EPR) measurements performed to evaluate very weak exchange interactions (defined as $\mathcal{H}_{ex}(i,j) = -J_{ij}\mathbf{S}_i\mathbf{S}_j$, with 10^{-3} cm$^{-1} < |J_{ij}| < 1$ cm^{-1}) between unpaired spins, transmitted through long and weak chemical pathways typical of protein structures. They are performed in appropriate model compounds, mainly copper derivatives of amino acids and peptides, making use of the phenomenon of exchange narrowing and collapse of the resonances. I describe the theoretical basis and the implementations of the method to different situations, including selected experimental values of the exchange couplings J between metal centers, and briefly discuss correlations between J and the structure of the paths. Results obtained in relatively simple EPR experiments performed at room temperature in single-crystal samples are compared with those obtained from thermodynamic magnetic measurements having higher experimental difficulties. The experimental information allows describing the role of molecular segments typical of biomolecules (H bonds, aromatic ring stacking, cation-π contacts, etc.) in the transmission of the exchange interaction. The values of J obtained in some model compounds are compared with those obtained in proteins to conclude that the magnitudes of the exchange interactions are useful to characterize long and weak biologically relevant chemical pathways. One observes that these exchange couplings are weakly dependent on the nature of the unpaired spins and strongly dependent on the chemical pathway. Thus, measurements of exchange couplings in model compounds may provide useful information about biological function, particularly about electron transfer in proteins.

1 Introduction

Metal ions or radicals with unpaired spins are coupled by dipolar and exchange interactions [1]. The anisotropic magnetic dipolar interactions carry geometric molecular information (distances and angles). They are transmitted through space and, in the point dipole approximation, have the predictable r^{-3} distance dependence [2]. Meanwhile, isotropic exchange interactions (often called "superexchange" [3]), are transmitted through the diamagnetic chemical bridges con-

necting the unpaired spins, and are strongly dependent on the electronic structure of the path [1, 3–5]. Their magnitude J is defined by*

$$\mathcal{H}_{ex} = -J\mathbf{S}_1\mathbf{S}_2, \tag{1}$$

where $\mathbf{S}_1$ and $\mathbf{S}_2$ are the spin operators of the unpaired electrons, and J carries information about the electronic wave functions of the path. $\mathcal{H}_{ex}$ is ferromagnetic (FM) when $J > 0$ and antiferromagnetic (AFM) when $J < 0$. Exchange interactions are usually evaluated from measurements of thermodynamic properties (magnetic susceptibility, magnetization, specific heat, etc.) [1, 6, 7]. Starting with the classical work of Bleaney and Bowers [8], electron paramagnetic resonance (EPR) has also played an important role in this direction [9].

The magnitude J of the exchange interaction can be calculated in terms of the electronic structure of the chemical pathway supporting the interaction. Since the work of Anderson [3], important theoretical advances have been made in this direction for simple pathways [1, 4, 5]. The explosive growth in recent years of the field of molecular magnetism has been supported by many experimental and theoretical efforts in order to measure and interpret the magnitudes of the exchange interactions [1]. Most of these efforts correspond to interactions having magnitudes $|J| \geq 1$ cm^{-1}.

The relevance of long and weak noncovalent chemical paths in protein structure and function has been widely discussed and accepted [10, 11]. They play important roles for electron transfer, molecular recognition, and in the bio-inspired chemical architecture in supramolecular chemistry, thus contributing to the function of the proteins. Characterizing these paths is difficult because they are generally combined with stronger covalent paths.

Many proteins and enzymes have in the ground state or in excited states of their biological cycle unpaired spins located in metal ions or in cofactor radicals. In many cases they interact through long pathways which determine the magnitude J of the exchange interaction. These values of J have been related to the matrix element for electron transfer between redox centers through the chemical path [12–18]. Thus, J is a useful parameter to characterize chemical pathways. Empirical results indicate that exponential dependence of J on path length gives reasonable agreement for groups of compounds with similar chemical bridges [19–21]. These findings are helpful to order the experimental information and to find trends helping to develop theoretical work on the difficult problem of exchange interactions transmitted through weak and long chemical bridges [1].

The weak interactions ($|J| < 1$ cm^{-1}) associated to long and complex chemical bridges are difficult to evaluate by standard thermodynamic techniques requiring sophisticated measurements at temperatures compatible with the interaction to be evaluated ($T < 1$ K; see, for example, ref. 22). Using EPR as a tool to determine dipolar and exchange interactions has been described by Bencini

---

* Other definitions are also used in the literature. We chose that of ref. 1 (eq. (1)), which is used throughout the paper. The values of J will be given in units of cm^{-1} (1 cm^{-1} = 1.4387 K = $2.998 \cdot 10^{10}$ s^{-1}).

and Gatteschi [9], who treated mainly the case of interactions larger than a few wave numbers in binuclear and polynuclear unpaired spin clusters. These methods integrate the wide range of EPR applications [23–25] and are important to deal with problems characteristic of molecular magnetism. However, in many cases they are not useful when dealing with very small exchange interactions.

This paper deals with EPR methods to evaluate extremely small exchange couplings, 10^{-3} cm$^{-1} < |J| < 1$ cm^{-1}, transmitted through chemical bridges of up to about 2.0 nm containing as much as about 13 diamagnetic atoms, as those encountered in weak chemical bridges of biological significance. The purpose is to call attention on this source of biological information provided by EPR and to review a method based on the theories of Anderson [26] and Kubo and Tomita [27] for exchange narrowing and collapse of magnetic resonances, which proved to be useful for this purpose. First I introduce basic ideas and illustrate the method with possible experiments. In later sections I review selected measurements in model compounds, mainly metal derivatives of amino acids and peptides resembling chemical bridges encountered in metalloproteins, that my group and other researchers have performed in recent years. I do not describe the experimental details, which can be found in the original references. However, I describe EPR measurements and analyses performed in a particular model compound, the copper complex of the amino acid glycine $[Cu(gly)_2]\cdot H_2O$ [28, 29], which may be helpful to understand the used procedures. Some EPR results in selected model compounds are compared with those obtained by classical thermodynamic techniques and with values obtained in proteins. The correlations between the values of J and the structure of the weak and long pathways supporting the exchange interactions, as well as the biological implications of our results, are discussed. I concentrate here on the isotropic exchange couplings and do not consider dipolar and other anisotropic magnetic couplings, which have been treated elsewhere [2, 9, 15, 16, 20, 25, 30] and are not directly related to the purpose of this work. A uniform notation is employed and we try to present a simpler and more compact description of the theoretical aspects than previous works.

2 EPR Spectra of Weakly Coupled Spin Systems

2.1 Binuclear and Polynuclear Units

Let us analyze first the EPR spectrum of a binuclear unit with two interacting spins 1/2, S_1 and S_2 (see ref. 30 for more details). The spin Hamiltonian is described by

$$\mathcal{H}_S = \mathcal{H}_Z + \mathcal{H}_{ex} + \mathcal{H}_{anis} = \mu_B \mathbf{B}_0 \left[\mathbf{g}_1\mathbf{S}_1 + \mathbf{g}_2\mathbf{S}_2\right] - J\mathbf{S}_1\mathbf{S}_2 + \mathcal{H}_{anis}. \qquad (2)$$

The first term on the right-hand side of Eq. (2) is the Zeeman interaction $\mathcal{H}_Z$, $\mathbf{g}_1$ and $\mathbf{g}_2$ are the g-tensors corresponding to $\mathbf{S}_1$ and $\mathbf{S}_2$, $\mathbf{B}_0 = \mu_0\mathbf{H}$ is the applied

magnetic field (μ_0 is the vacuum permeability) and μ_B is the Bohr magneton. The second term is the exchange interaction between $\mathbf{S}_1$ and $\mathbf{S}_2$ (Eq. (1)), and $\mathcal{H}_{anis}$ contains dipolar and other anisotropic interactions.

If the two spins are identical, $\mathbf{g}_1 = \mathbf{g}_2 = \mathbf{g}$, and the Zeeman term $\mathcal{H}_Z = \mu_B \mathbf{B}_0 \mathbf{g} [\mathbf{S}_1 + \mathbf{S}_2]$ commutes with the exchange interaction term $\mathcal{H}_{ex}$. In that case and when $\mathcal{H}_{anis}$ is negligible, the EPR spectrum of the binuclear unit is independent of J and equal to the single resonance corresponding to each individual spin. When $\mathcal{H}_{anis}$ is not negligible, it produces a splitting of the single line which varies with the orientation of the magnetic field. This is the case observed for the classical copper acetate hydrate, having identical copper ions in centro-symmetric binuclear units [31], where no information about J is obtained from the shape of the spectra, but from their temperature variation produced by changes in the level populations. It is possible to evaluate J if the EPR spectra are obtained as a function of temperature for $T \leq |J|/k_B$ or $T \leq g\mu_B B_0/k_B$, a very low temperature for weak exchange interactions and for the microwave frequencies of standard EPR spectrometers (however, see, for example, ref. 16). In order to evaluate J from the EPR spectrum of a weakly coupled binuclear unit, the spins should have different g-values.

One defines the ratio $x = |J|/\Delta$, between the exchange coupling $|J|$ and the difference $\Delta = |g_1 - g_2|\mu_B B_0$ between the Zeeman energies of $\mathbf{S}_1$ and $\mathbf{S}_2$ ($g_i = (\mathbf{h}\mathbf{g}_i\mathbf{g}_i\mathbf{h})^{1/2}$, where $\mathbf{h} = \mathbf{B}_0/|\mathbf{B}_0|$ is the direction of the applied magnetic field). Figure 1, obtained with the EasySpin EPR spectra simulation package [32], displays the absorption spectrum of a binuclear unit with g-factors g_1 and g_2 for a

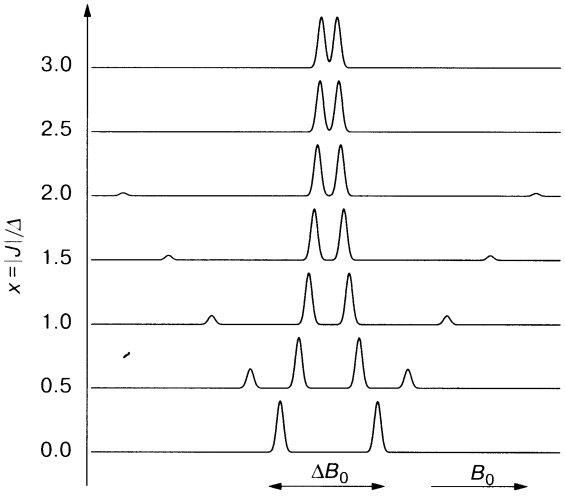

Fig. 1. Calculated EPR absorption $\chi''(B_0)$ of a binuclear unit of two spins 1/2 with different g-factors, as a function of the ratio $x = |J|/\Delta$ between the exchange coupling J and the difference Δ between the Zeeman energies of the two spins. Anisotropic interactions between spins are neglected (see text).

given orientation of $\mathbf{B}_0$ as a function of x. For $x = 0$, Fig. 1 shows two resonances with a magnetic field splitting $\Delta B_0 \sim (|g_1 - g_2|/(g^2\mu_B))\hbar\omega_0$ ($\hbar\omega_0$ is the energy of the microwave employed in the experiments and $g = 1/2(g_1 + g_2)$ is the average g-factor). As x increases, these resonances asymptotically collapse to the average g-value. Simultaneously, two resonances whose amplitudes decrease with increasing x, come apart from the central doublet and disappear for $x \gg 1$. This general behavior does not depend on the sign of J, except on the labeling of the resonances. The asymptotic collapse of the signals allows measuring exchange couplings with magnitudes $|J| \sim \Delta$, a small fraction of the energy of the employed microwave, when the splitting ΔB_0 in the absence of exchange can be predicted. This method was applied to evaluate an exchange coupling $|J| = 0.21(2)$ cm^{-1} between a Cu(II) ion replacing the Fe(II) ion in reaction centers of photosynthetic bacteria and the reduced quinone acceptor $Q_A^{\bullet -}$ at about 0.9 nm [33]. In that case the dipolar coupling between Cu(II) and $Q_A^{\bullet -}$ and the hyperfine interaction of Cu(II) were also considered. Also, since the unpaired spin in $Q_A^{\bullet -}$ is generated for the EPR experiment, the spectrum of the Cu(II) ion was measured in the absence and in the presence of the exchange coupling [33].

The great advantage of the process described in Fig. 1 is that experiments at low temperatures are not required in order to evaluate small interactions, as it occurs with the thermodynamic experiments. However, studying binuclear (or polynuclear) units with this method requires very weak couplings between binuclear units and becomes complicate when g_1 and g_2 are very similar, or when oriented single-crystal samples are not available. In addition, anisotropic contributions to the interaction between the spins (dipolar and anisotropic exchange) play a dominant role in the shape of the spectrum, masking the effects of larger isotropic exchange interactions [15, 16]. The case of polynuclear units can be treated in a similar way and since the corresponding spin Hamiltonians are finite, they can be solved exactly. The exchange interactions in many binuclear or polynuclear unpaired spin units in proteins have been studied.

2.2 Three-Dimensional Magnetic Model Systems

Several types of problems make it sometimes difficult or impossible to evaluate weak exchange interactions between unpaired spins for binuclear and polynuclear units in proteins. They are mainly problems with the samples (availability of single crystals, presence of other magnetic ions or of impurities, etc.), or with the characteristics of the EPR spectra (large anisotropic contributions, similar g-values, etc.). These problems favor the possibility of studying model compounds containing chemical bridges similar to those occurring in the biomolecules. With this purpose in mind we have chosen metal derivatives of amino acids and peptides which can be crystallized and detailed single-crystal EPR experiments can be performed in pure compounds. They have translational symmetry and in many cases are magnetically three-dimensional (3-D). Instead of studying weakly coupled binuclear or polynuclear units with small differences in the g-factors, one

studies model compounds having metal ions with anisotropic g-factors in two or more symmetry-related (rotated) sites in the unit cell, connected by appropriate chemical pathways. In some cases the model compounds can be chemically designed to provide convenient pathways. It will be shown that, considering the crystallographic symmetry properties of the samples, these methods allow evaluating selectively exchange interactions acting simultaneously between the metal ions in the exchange network, even when their magnitudes differ by as much as two or three orders of magnitude.

The spin Hamiltonian of a crystalline sample containing unpaired spins in two symmetry-related sites, A and B, coupled by exchange interactions and in the presence of B_0 is given by

$$\mathcal{H} = \mathcal{H}_z + \mathcal{H}_{ex} + \mathcal{H}_{anis} = \mu_B \mathbf{B}_0(\mathbf{g}_A \mathbf{S}_A + \mathbf{g}_B \mathbf{S}_B) - \sum_{i \neq j} J_{iA,jA} \mathbf{S}_{iA} \mathbf{S}_{jA} - \sum_{i \neq j} J_{iB,jB} \mathbf{S}_{iB} \mathbf{S}_{jB} - \sum_{i,j} J_{iA,jB} \mathbf{S}_{iA} \mathbf{S}_{jB} + \mathcal{H}_{anis} \quad (3)$$

with $\mathbf{S}_A = \sum_i \mathbf{S}_{iA}$ and $\mathbf{S}_B = \sum_i \mathbf{S}_{iB}$, where $\mathbf{S}_{iA}$ and $\mathbf{S}_{iB}$ are the spin operators corresponding to metal ions in lattice sites A and B of the ith unit cell. $\mathcal{H}_z$ is the Zeeman interaction and $\mathcal{H}_{ex}$ contains the isotropic exchange interactions between the spins in the lattice. The anisotropic contributions included in $\mathcal{H}_{anis}$ are neglected for our purpose. It is not possible to obtain an exact solution allowing to calculate the EPR spectra of this many-particle system, as in the case of binuclear or polynuclear units, and the problem has been solved under different approximations. The simplest method is using the generalized Bloch equations [20, 25, 34, 35]. Another approach is the stochastic theory proposed by Anderson [26], which is physically appealing and provides a basic explanation of the phenomena, keeping reasonable theoretical simplicity. It only accounts for the effects of the adiabatic terms. A quantum approach to the problem is the perturbative formalism of Kubo and Tomita [27], which may include the influence of nonadiabatic terms and allows a wider group of applications in order to evaluate exchange interactions (for a basic description, see ref. 36, chapt. 7). The results of the theories of Anderson [26] and Kubo and Tomita [27] have been used extensively in magnetic resonance (EPR and nuclear magnetic resonance [NMR]) in the problem of motional narrowing. The problem of exchange narrowing and collapse, which is important in EPR, has received less attention (however, see early work in ref. 37). Applications of the general theories [26, 27] to determine exchange interactions reported previously by us [38–40] are summarized below. These applications have the advantage that the contributions to the EPR spectra of anisotropic interactions, which complicate the study of exchange interactions in isolated binuclear or polynuclear clusters, tend to be averaged out by the exchange in a 3-D magnetic compound. In cases where the Bloch equations and the methods of Anderson [26] and Kubo and Tomita [27] have been applied to the same system, similar results have been obtained.

Within Anderson's model [26] and in the absence of exchange, the shape of the resonances is assumed to be Gaussian. The exchange introduces a random

jumping between a finite set of allowed frequencies corresponding to resonance lines in an assumed stationary Markovian process [26, 27, 41]. This random process arises from the distribution of magnitudes of the exchange coupling in a solid with an infinite number of interacting spins and its effect is different from the behavior of a binuclear unit. The random spin dynamics introduced by the exchange is described by a spin correlation time τ_{cx} and by the associated exchange frequency $\omega_{cx} = 2\pi/\tau_{cx}$. The value of ω_{cx} has to be related by a more detailed theory to the exchange interactions coupling the spin system ($\mathcal{H}_{ex}$ in Eq. (3)).

Figure 2a shows the evolution of the spectrum of two mingled families of different spins 1/2 as a function of $x = \omega_{cx}/\Delta\omega$, where $\Delta\omega = \Delta/\hbar$ is the distance in frequency units between the resonances corresponding to each family in the absence of exchange coupling. For $x = 0$, one observes two resonances with a magnetic field splitting $\Delta B_0 = \Delta/g\mu_B$. When x increases, the resonances broaden and merge to a central position, where they collapse to a single broad reso-

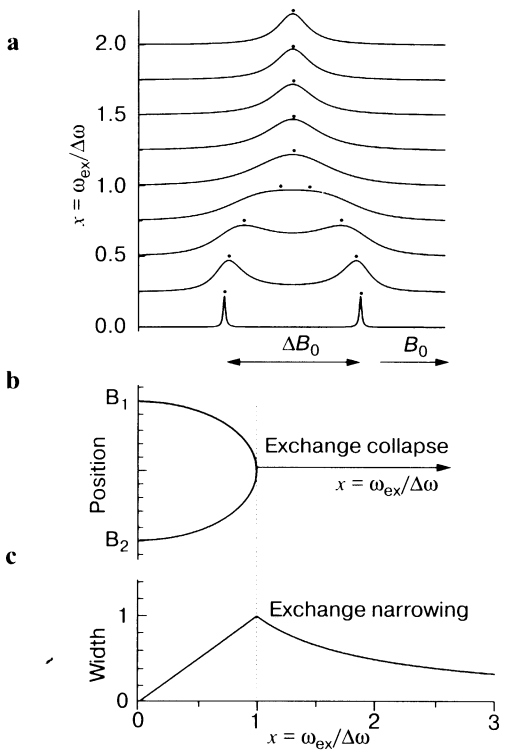

Fig. 2. Description of the phenomenon of exchange narrowing and collapse using Anderson's theory [26] for a compound with two types of spins 1/2 interacting through isotropic exchange. The parameter $x = \omega_{cx}/\Delta\omega$ is the ratio between the exchange frequency ω_{cx} and the difference $\Delta\omega$ between the Zeeman energies of the spins in angular frequency units, calculated from the molecular g-values. **a** EPR absorption $\chi''(B)$. The dots on top of the signals indicate their centers. **b** Position of the signals, as obtained from **a**, as a function of x. **c** Width of the signals, as obtained from **a** as a function of x.

nance for $x = 1$. This collapse is a phenomenon different from the asymptotic convergence observed for binuclear or polynuclear units (compare Figs. 1 and 2a). For $x > 1$, the collapsed resonance narrows again with increasing x and tends to have a Lorentzian line shape interpreted as the superposition of a narrow and a wide resonance [26]. Two ranges of x are defined by Fig. 2. For $x < 1$ ($\omega_{ex} < \Delta\omega$), one observes the resolved resonances regime, with two resonances. The centers of the collapsing resonances in Fig. 2a are indicated by dots, and their positions and widths are displayed in Fig. 2b and c as a function of x. For $x > 1$, in the collapsed resonances regime, one observes a single resonance at the average position that narrows with increasing x. Within the Kubo and Tomita's theory [27], the analysis of each regime requires a different perturbative approximation.

In single-crystal samples with differently oriented metal sites in the unit cell, the value of $x = \omega_{ex}/\Delta\omega$ can be varied by changing $\Delta\omega$ with the microwave frequency or with the orientation of the magnetic field. Figure 3 (modified from ref. 28) displays the observed normalized splitting of the resonances as a function of $1/\Delta\omega$ and reproduces experimentally the predictions of Anderson's theory [26] by changing $\Delta\omega$ with the orientation of $\mathbf{B}_0$. This experimental result displays the behavior described by Anderson [26] and allowed to evaluate exchange interactions between neighbor copper ions in $[Cu(gly)_2] \cdot H_2O$ (see Sect. 4). Simi-

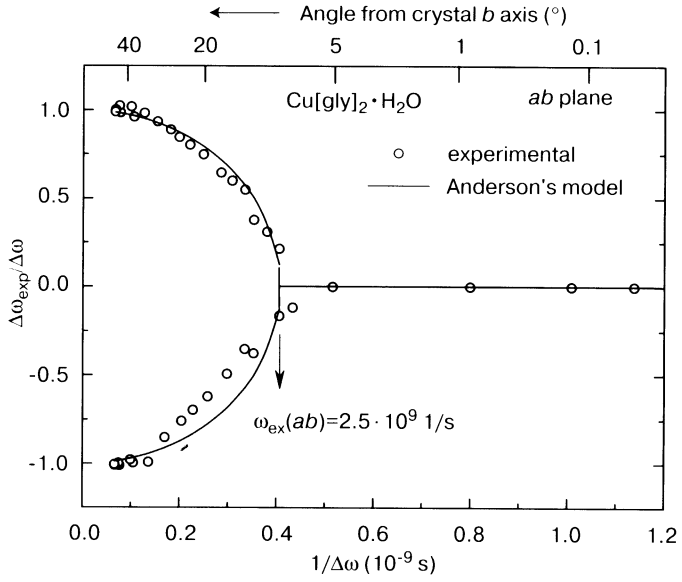

Fig. 3. Experimental evidence of the collapse of the EPR signals of two unpaired spins with different g-factors. The ratio between the observed and the calculated splitting of the resonances as a function of the reciprocal of the difference between their Zeeman energies in frequency units, which is varied with the orientation of the magnetic field. The upper horizontal axis displays the angular displacement from the crystal axis.

lar experiments were performed for Cu(L-isoleucine)$_2$ [42]. To study the widths of the signals, we describe first a simple procedure following Anderson's ideas [26] that predicts the basic results. To evaluate J, it is more convenient to use the theory of Kubo and Tomita [27, 37].

3 Theoretical Basis

3.1 Collapsed-Resonance Regime

Due to the anisotropy of the g-tensors, compounds with two or four symmetry-related metal sites display separate resonance lines for an arbitrary orientation of the magnetic field. In the case of Cu(II) ions having g-factors varying from $g_{\parallel} \sim 2.25$ to $g_{\perp} \sim 2.05$ (see ref. 24, sect. 3.5) it is $\Delta g/g \leq 0.1$, the differences in their Zeeman energies are $\Delta \leq 0.1\hbar\omega_0$ and the magnetic field splittings are $\Delta B_0 \leq 0.1\ \hbar\omega_0/g\mu_B$. The exchange interactions produce a spin dynamics with a characteristic frequency ω_{ex} that averages out the splitting of the lines. Cases where $x > 1$ allow simple implementations of the exchange narrowing process to evaluate exchange interactions [38, 43–54].

When the model compound has metal ions in two sites A and B related by a proper rotation, we define the spin operators

$$\mathbf{S} = \mathbf{S}_A + \mathbf{S}_B = \sum_i (\mathbf{S}_{iA} + \mathbf{S}_{iB}) \quad \text{and} \quad \mathbf{s} = \mathbf{S}_A - \mathbf{S}_B = \sum_i (\mathbf{S}_{iA} - \mathbf{S}_{iB}), \tag{4}$$

which allows writing the Zeeman contribution to the spin Hamiltonian of Eq. (3) as

$$\mathcal{H}_z = \mathcal{H}_z^0 + \mathcal{H}_z' = \mu_B \mathbf{B}_0 \mathbf{g} \mathbf{S} + \mu_B \mathbf{B}_0 \mathbf{G} \mathbf{S},$$

where

$$\mathbf{g} = 1/2(\mathbf{g}_A + \mathbf{g}_B) \quad \text{and} \quad \mathbf{G} = 1/2(\mathbf{g}_A - \mathbf{g}_B). \tag{5}$$

If the anisotropy of the molecular g-tensors $\mathbf{g}_A$ and $\mathbf{g}_B$ is small, $\mathbf{G}$ is small and $\mathcal{H}_z' \ll \mathcal{H}_0$. The exchange coupling of Eq. (3) commutes with the total spin $\mathbf{S}$ and thus with $\mathcal{H}_z^0$, but not with $\mathbf{s}$ and $\mathcal{H}_z'$. Thus, the exchange interactions introduce a stochastic time modulation of $\mathcal{H}_z'$ that averages it out for large x. When $x = 0$, one observes two lines with g-factors $g_A = (\mathbf{h}\mathbf{g}_A\mathbf{g}_A\mathbf{h})^{1/2}$ and $g_B = (\mathbf{h}\mathbf{g}_B\mathbf{g}_B\mathbf{h})^{1/2}$, where $\mathbf{h} = \mathbf{B}_0/|\mathbf{B}_0|$. For $x > 1$, there is a single resonance with g-tensor g as shown by Fig. 2. The EPR line width changes as a result of this averaging out process of $\mathcal{H}_z'$ produced by $\mathcal{H}_{ex}$ [38, 40]. To analyze that, one diagonalizes $\mathcal{H}_z^0$ choosing $\boldsymbol{\zeta} = \mathbf{gh}/|\mathbf{gh}|$ as the quantization axis. In this basis

$$\mathcal{H}_z^0 = g\mu_B B_0 S_\zeta \quad \text{and} \quad \mathcal{H}_z' = \mu_B B_0 (\mathbf{Gh})_\zeta s_\zeta + \mu_B B_0 (\mathbf{Gh})_\perp s_\perp. \tag{6}$$

The first contribution to $\mathcal{H}_z'$ is the diagonal "residual Zeeman term". The second contribution is nondiagonal, and generally neglected (however, see below). Thus,

$$\mathcal{H}_z'(\text{sec}) = \mu_B B_0 (\mathbf{Gh})_\zeta s_\zeta = \Gamma \mu_B B_0 s_\zeta \quad \text{with} \quad \Gamma = \frac{\mathbf{hgGh}}{(\mathbf{hggh})^{1/2}} \tag{7}$$

is the secular contribution to the perturbation acting on the Hamiltonian

$$\mathcal{H}_0 = g\mu_B B_0 S_\zeta + \mathcal{H}_{ex}.$$

Within Anderson's model the width ΔB of the collapsed signal for $x > 1$ is proportional to the second moment of the residual Zeeman term divided by the exchange frequency ω_{ex} associated to $\mathcal{H}_z'(\text{sec})$:

$$\Delta B = \frac{1}{g\mu_B} \frac{\left\langle [\mathcal{H}_z'(\text{sec})]^2 \right\rangle}{\hbar\omega_{ex}} \propto \frac{1}{g\mu_B} \frac{(\mathbf{hgGh})^2}{g^2\hbar\omega_{ex}} (\mu_B B_0)^2 = \frac{1}{g\mu_B} \frac{(\mathbf{hgGh})^2}{g^4\omega_{ex}} \hbar\omega_0^2,$$

where ω_0 is the angular microwave frequency and ω_{ex} is associated to the time correlation function of s_ζ (Eqs. (4) and (7)) when modulated by the exchange. For small g-anisotropy G (Eq. (5)), it is

$$(\mathbf{hgGh})^2 \approx g^2 (\mathbf{hGh})^2 = \frac{g^2 [\mathbf{h}(\mathbf{g}_A - \mathbf{g}_B)\mathbf{h}]^2}{4} = \frac{g^2 [g_A(\theta,\phi) - g_B(\theta,\phi)]^2}{4}.$$

Thus

$$\Delta B \propto \frac{[g_A(\theta,\phi) - g_B(\theta,\phi)]^2 \hbar\omega_0^2}{4g^3(\theta,\phi)\mu_B\omega_{ex}}. \tag{8}$$

To relate the exchange frequency ω_{ex} to the exchange coupling parameters introduced in Eq. (3), a quantum calculation is needed. We used the perturbative theory of Kubo and Tomita defining $\mathcal{H}_0 = \mathcal{H}_z^0 + \mathcal{H}_{ex}$ as the unperturbed Hamiltonian, and $\mathcal{H}_z'(\text{sec})$ as the perturbation. The peak-to-peak EPR line width calculated by Kubo's stochastic formalism [38, 40] is

$$\Delta B_{pp}(\theta,\phi) = \sqrt{\frac{2\pi}{3}} \frac{(g_A(\theta,\phi) - g_B(\theta,\phi))^2 \omega_0^2 \hbar}{4g^3(\theta,\phi)\mu_B\omega_{ex}}, \tag{9}$$

where the factor $(2\pi/3)^{1/2}$ considers that one measures the peak-to-peak width. According to this calculation, which assumes Gaussian behavior of the correla-

tion function of s, the exchange frequency ω_{ex} is related to the exchange interactions in Eq. (3) by [38 40]:

$$\omega_{ex}^2 = 4S(S+1)\frac{\left[\sum_i Z_i J_i^2\right]}{3\hbar^2}, \tag{10}$$

where S is the spin of the metal ion and J_i are the magnitudes of the exchange interactions between a metal ion in site A and metal ions in neighboring sites B_i. The index i considers different B-type neighbors in the 3-D lattice and Z_i is the number of neighbors type B_i for a metal site type A. Because of the square power in the values of J_i in Eq. (10), one needs in general to consider only first neighbors. Equation (9) shows a dependence of the width on ω_0^2, and an angular dependence proportional to the square of the difference between the molecular g-factors of the collapsing sites. It is similar to what is obtained with the simpler Anderson theory (Eq. (8)) and has been used in several works to calculate exchange interactions from line width data [28, 38–40, 42–55].

In some cases the crystal structure of the model compound contains four metal sites in the unit cell labeled as A, B, C and D related by rotations around the crystal axes. There are exchange couplings connecting the spins in different pairs of sites (AA, AB, AC, AD and symmetry-related pairs) and one wants to obtain the magnitudes of the parameters J_{AB}, J_{AC} and J_{AD} coupling a spin in site A with spins in sites B, C and D from the EPR measurements. Each exchange coupling parameter is associated to a specific chemical path that can be identified in the crystal structure of the compound. The general ideas for these cases follow those described for metal ions in two sites, considering in addition the symmetry relations between the sites [40]. Four symmetry combinations of the spin variables $\mathbf{S}_A$, $\mathbf{S}_B$, $\mathbf{S}_C$ and $\mathbf{S}_D$ are defined. One is the total spin $\mathbf{S}$, which is not affected by the exchange interaction. The other three, called $\mathbf{s}_u$ (u = 1, 2, 3), give rise to three residual Zeeman terms defining three exchange frequencies $\omega_{ex}(u)$ when randomly modulated by the exchange. Since the $\mathbf{s}_u$ operators are defined using symmetry conditions [40], when the line width measurements are performed in the crystal planes of the sample, the data in each plane are usually related to only one of the exchange frequencies. In that case one can label each ω_{ex} with the name of the plane.

In cases when the magnitudes of the exchange couplings have very different magnitudes, they are related to the exchange couplings by relations similar to Eq. (10), specific for each $\mathbf{s}_u$. When the magnitudes of the couplings J are similar, higher-order contributions and nonsecular terms (see Eq. (6)) could complicate formally the problem. Still, there is not yet a fully satisfying result for the relation between the exchange frequencies $\omega_{ex}(u)$ and the magnitudes of the exchange couplings when J_{AB}, J_{AC} and J_{AD} have similar magnitudes. The basic theory leading to Eqs. (9) and (10) is described in ref. 40 and has been applied to several specific cases in refs. 28, 39, 42, 50–54. The EPR spectrum allows evaluating simultaneously up to three exchange frequencies related to

the relevant exchange couplings in the magnetic network of the model compound. They provide information about these couplings particularly in cases when they have magnitudes differing up to two or three orders of magnitude. In these cases, EPR in single-crystal samples provides a unique technique to evaluate exchange interactions acting simultaneously and having very different magnitudes.

When the EPR measurements are performed at different microwave frequencies ω_0, the dependence of Eq. (9) on ω_0^2 allows the separation of contributions to the width arising from the exchange narrowing process from those arising from dipolar and other interactions that are frequency independent (see for example, refs. 28, 42–49). The molecular g-tensors $\mathbf{g}_A$ and $\mathbf{g}_B$ corresponding to individual metal sites can be evaluated under simple assumptions [56, 57] from the crystal g-tensor obtained from the observed resonance positions and the value of ω_{ex} is calculated by Eq. (9) from line width measurements in single-crystal samples. A similar procedure can be used for the case of four metal sites in the unit cell. Using this method, magnitudes of J between 0.001 and 1 cm^{-1} can be evaluated by standard EPR line width measurements performed at 9 and 35 GHz, at room temperature. It is only possible to evaluate exchange interactions between metal ions in different (rotated) lattice sites (e.g., J_{AB}, in the description above). One cannot evaluate J_{AA} between metal sites related by a lattice translation because it operates between identical spins and does not contribute to the spectrum.

3.2 Resolved-Resonance Regime and Crossing between Regimes

The most straightforward measurement in the resolved-resonance regime is described by Fig. 3. One follows the collapse of the signal by changing the Zeeman splitting $\Delta\omega$ with magnetic field rotation. This gives a direct measurement of the exchange frequency producing the collapse. As observed in several previous works [28, 49, 54], the line width of the collapsed resonances in cases where one crosses from a collapsed-resonance regime to a resolved regime allows measuring very small exchange interactions using Eq. (9). Since the angular variation is performed in a narrow angular range, other contributions to the width remain constant, and the measurements of small values of J (ca. 10^{-3} cm^{-1}) are very precise (see below).

4 Specific Example: $[Cu(gly)_2] \cdot H_2O$

To illustrate the procedures described above, I review experimental results reported by Martino et al. [28] for the copper complex of glycine and emphasize the general aspects of the problem. They are appropriate for this purpose because they display most characteristics emphasized in this review. This compound was also studied by Hoffmann et al. [29], who used the Bloch equations method to analyze the data. More details can be found in the original articles.

4.1 Structure and Exchange Pathways in $[Cu(gly)_2]\cdot H_2O$

The structure of *cis*-aqua-bis(glycinato-N,O)-copper(II) ($C_4H_{10}CuN_2O_5$, named here $[Cu(gly)_2]\cdot H_2O$) was solved early by Tomita and Nitta [58] and Freeman et al. [58] and recently by Moussa et al. [60] and Casari et al. [61]. At the time the EPR study of $[Cu(gly)_2]\cdot H_2O$ by Martino et al. [28] was published, the available structural results were those of Freeman et al. [59], which did not include the protons in the lattice. Here we discuss the magnetic data using the recent crystallographic results of Casari et al. [61], which include the protons, allowing a better description of the H bonds. For consistency, we adapt the labeling of the atoms, the definition of the unit cell parameters and the symmetry operations of Casari et al. [61] to those of Freeman et al. [59].

$[Cu(gly)_2]\cdot H_2O$ crystallizes in the space group $P2_12_12_1$ with lattice parameters a = 1.06850(3) nm, b = 0.51920(1) nm, and c = 1.35535(4) nm and 4 molecules in the unit cell (Z = 4) [61]. The unit cell of the structure shown in Fig. 4 includes the labeling of the non-H atoms. The Cu ion is in a noncentro-symmetric approximately square planar *cis* configuration with oxygen ligands O-1 and O-3 at 0.1955 nm, and nitrogen ligands N-1 and N-2 at 0.1996 and 0.2007 nm, respectively. An elongated octahedral coordination of the Cu ion is completed with the oxygen O-5 from the water molecule at 0.2373 nm, and the carboxylate oxygen O-2 of an adjacent molecule at 0.2656 nm (a weak connection shown with a thinner line in Fig. 4). The distance from the copper ion to the apical water oxygen O-5 is short (d = 0.2373 nm) for this weakly covalent bond. The intermolecular stability is provided by five types of H bonds. The shortest ones, between O-5 and O-2 (type I, d = 0.2759 nm, α = 170.3°) and between O-5 and O-4 (type II, d = 0.2803 nm, α = 170.8°), involve the water protons. Other intermolecular H bonds exist between N-1 and O-4 (type III,

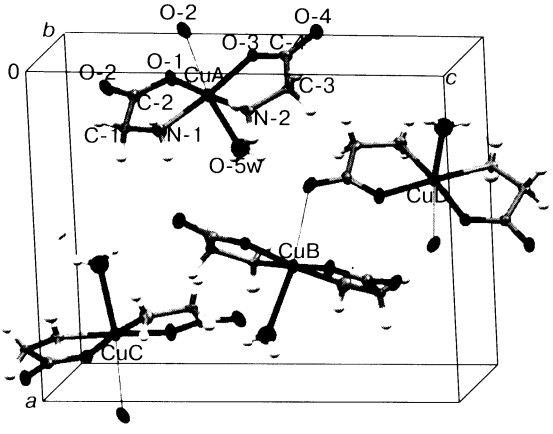

Fig. 4. Unit cell of $[Cu(gly)_2]\cdot H_2O$ according to ref. 61. The unit cell axes and the labeling of the atoms were chosen as in ref. 59.

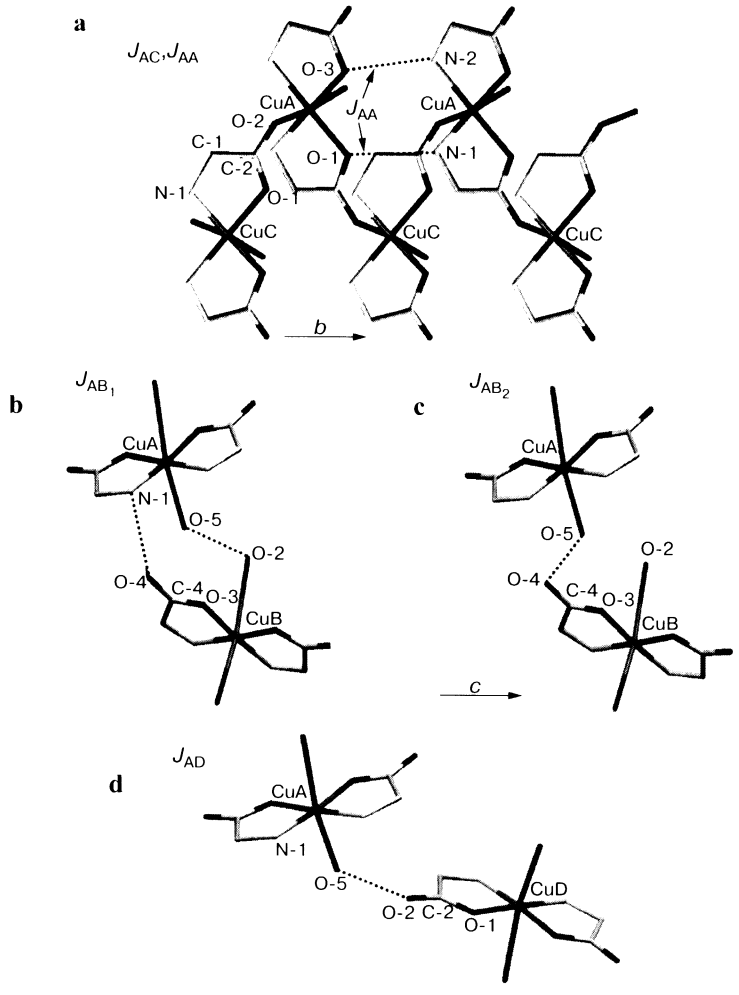

Fig. 5. Superexchange pathways in $[Cu(gly)_2]\cdot H_2O$ obtained from the crystallographic information [61] and described in the text.

$d = 0.2951$ nm, $\alpha = 170.8°$), between N-1 and O-1 (type IV, $d = 0.2992$ nm, $\alpha = 159.6°$) and between N-2 and O-3 (type V, $d = 0.3093$ nm, $\alpha = 159.4°$). An equatorial-apical carboxylate bond connecting the Cu atoms and the H bonds also provide intermolecular interactions and superexchange pathways between Cu ions in $[Cu(gly)_2]\cdot H_2O$.

According to the space group of $[Cu(gly)_2]\cdot H_2O$, for each molecule type A in (x,y,z), there are molecules B, C and D at $(1/2 + x, 1/2 - y, -z)$, $(-x, 1/2 + y, 1/2 - z)$, $(1/2 - x, -y, 1/2 + z)$, related by C_2 rotations around the axes a, b and c, respectively, plus translations (Fig. 4). The pathways between copper neighboring pairs A–A, A–B, A–C and A–D are obtained from the crystal data.

Equatorial-apical carboxylate bonds O-1–C-2–O-2 between neighboring Cu ions in A and C sites (named CuA and CuC) give rise to weakly coupled spiral Cu chains along the *b*-axis (Fig. 5a). The distance between neighboring CuA and CuC ions (or CuB and CuD) in the chain is 0.5319 nm and that measured along the carboxylate bridge is 0.7133 nm. A CuA is coupled to two neighboring CuC at both sides in the chain through these carboxylate pathways that support an intrachain exchange coupling J_{AC}. A CuA is also connected to two similar CuA at both sides along the chain at a distance $b = 0.5192$ nm through H bonds types IV and V (Fig. 5a), connecting equatorial ligands to Cu with bond lengths of 0.699 and 0.708 nm, respectively. There are two types of chains containing CuA and CuC, and CuB and CuD ions, respectively, related by C_2 rotations around the *a*- or *c*-axes. A type AC chain is coupled to four neighboring BD chains. A CuA ion is connected to four nearest neighboring CuB in two of these BD chains through two different A–B pathways, sketched in Fig. 5b and c, supporting couplings J_{AB_1} and J_{AB_2}. There are two pathways supporting J_{AB_1} between a CuA and two CuB ions at 0.6053 nm, each containing two bridges; one is CuA–O-5–H···O-2–CuB with a H bond type I between the apical ligands (total bond length of 0.7797 nm); the other bridge contains a H bond type III (N-1–H···O-4) and the carboxylate bond O-4–C-4–O-3, CuA–N-1–H···O-4–C-4–O-3–Cu-B, with 5 diamagnetic atoms and a total bond length of 0.9416 nm. Path AB_2 connecting coppers at 0.7371 nm with a total length of 0.9651 nm contains a H bond type II, connecting the apical oxygens of two coppers CuA–O-5–H···O-4–CuB. A CuA is connected to two CuD at 0.7652 nm in neighboring chains with a coupling J_{AD} supported by a pathway containing a H bond O-5–H···O-2 and a carboxylate bridge O-4–C-4–O-3, with a total length of 0.9620 nm (Fig. 5d). This detailed description of the exchange pathways shows the complexity of the magnetic network that one tries to solve by EPR.

4.2 EPR Results and Analysis for $[Cu(gly)_2]\cdot H_2O$

As a consequence of the symmetry relations in the $P2_12_12_1$ space group of $[Cu(gly)_2]\cdot H_2O$, the resonances corresponding to CuA and CuC ions (and CuB and CuD) should be coincident in the *ac* plane. Also, those of CuA and CuB ions (and CuC and CuD) should be coincident in the *bc* plane. Also, the resonances corresponding to CuA and CuD (and CuB and CuC) should be coincident for $\mathbf{B}_0$ in the *ab* crystal plane. Two resonances should be observed for $\mathbf{B}_0$ in the crystallographic planes. The resonances of all four sites are coincident by symmetry for $\mathbf{B}_0$ along the crystal axes.

The values of g^2 observed by Martino et al. [28] at 9.7 and 33 GHz with the magnetic field in the crystal planes *ab*, *ac* and *bc* of a sample of $[Cu(gly)_2]\cdot H_2O$ are shown in Fig. 6. A single resonance is observed at both frequencies in the *ac* and *bc* planes. Two resonances are observed for most orientations in the *ab* plane, except for $\mathbf{B}_0$ close to the crystal axes, where they collapse to one resonance. The

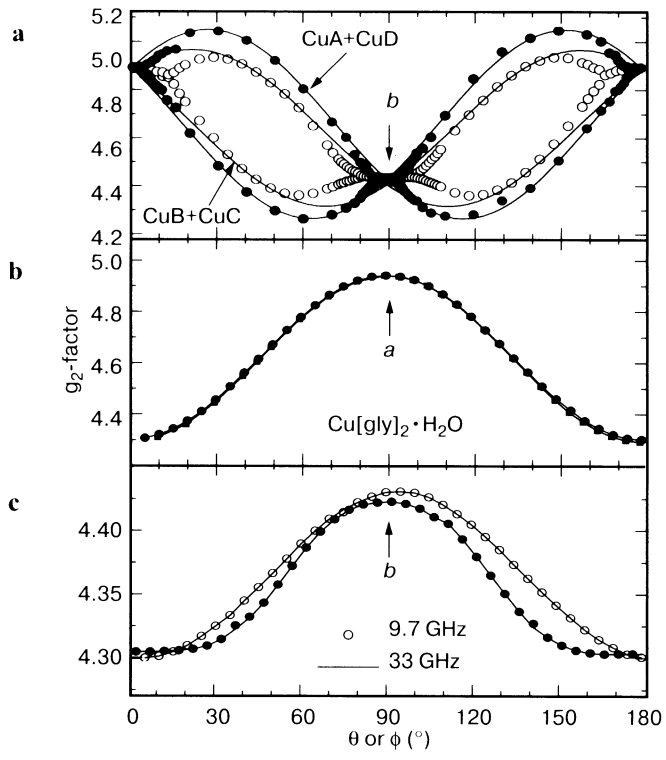

Fig. 6. Values of g^2 observed at two microwave frequencies with the magnetic field B_0 in three orthogonal planes of single crystals of $[Cu(gly)_2] \cdot H_2O$ [28]. **a** *ab* plane, **b** *ac* plane and **c** *bc* plane. The solid lines are obtained from the values of the components of the g^2 tensor (see ref. 28). The differences between the results at the two microwave frequencies are attributed to nonsecular contributions to the Zeeman terms.

values of g^2 observed in the three crystal planes displayed in Fig. 6 allow calculating two crystal g^2 tensors, corresponding to the two sets of resonances. Also, making simple assumptions [28, 56, 57], the molecular g-tensors $\mathbf{g}_A$, $\mathbf{g}_B$, $\mathbf{g}_C$ and $\mathbf{g}_D$ corresponding to Cu ions in the four lattice sites can be calculated from the crystal g-tensors [28].

The results in Fig. 6 indicate that the exchange frequency $\omega_{ex}(ac)$ is larger than the Zeeman splitting between neighboring CuA and CuB (or CuA and CuD) for any direction in the *ac* plane. Also, $\omega_{ex}(bc)$ acting for $\mathbf{B}_0$ in the *bc* plane is larger than the Zeeman splitting between neighboring CuA and CuC (equal to that between CuA and CuD) at both microwave frequencies and any magnetic field direction. Observing two resonances in most orientations of the *ab* plane indicates that the exchange frequency $\omega_{ex}(ab)$ acting in this plane can produce the collapse of the resonances of neighboring CuA and CuB (or CuA and CuC) only for $\mathbf{B}_0$ close to the crystal axes, where the Zeeman splitting $\Delta\omega$ is small. These conditions are related to both the exchange frequencies and the Zeeman

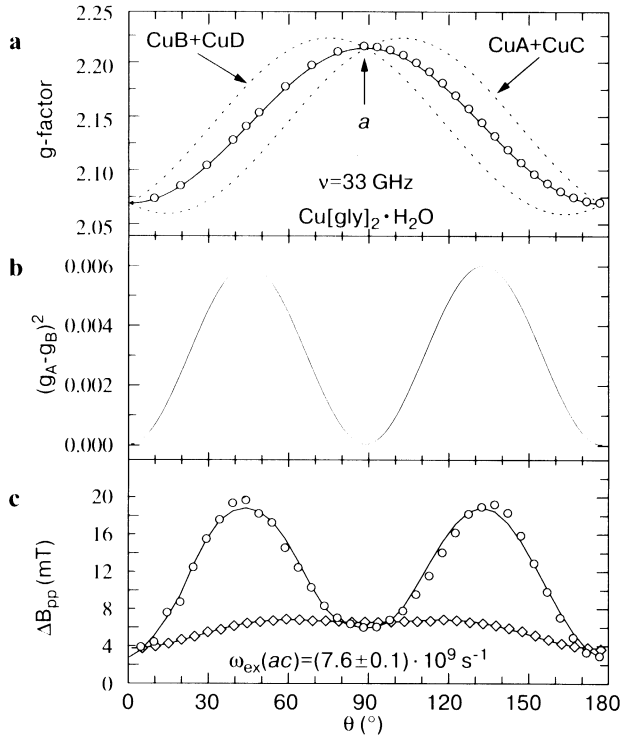

Fig. 7. **a** g-values of the resonance line observed for B_0 in the ac plane (circles) [28]. The dotted lines display the angular variation calculated for the molecular g-values. **b** Square of the difference between the molecular g-values plotted in **a**. **c** Peak-to-peak line width observed at 9.7 (◇) and 33 (○) GHz in the ac plane. The solid lines were obtained by fitting Eq. (9) to the data [27].

splitting in the crystal planes. Figures 7a and 8a display the g-values of the single lines observed at 33 GHz and those calculated for the molecular tensors $\mathbf{g}_A$, $\mathbf{g}_B$, $\mathbf{g}_C$ and $\mathbf{g}_D$, for the magnetic field in the ac and bc planes, respectively. As expected, the g-value of the collapsed resonance is the average of those calculated for the molecular g-tensors. Figure 9a displays the observed g values of the two resonances in the ab plane (circles) at 33 GHz, and those calculated with the molecular g-tensors obtained from the data (lines). Figures 7b, 8b and 9b display the calculated squares of the differences between these molecular g-factors in the three planes. In the case of Fig. 9b (ab plane), it includes only the region close to the b-axis where one line is observed. These results are needed to model the line width data (see Eq. (9)). The circles in Figs. 7c, 8c and 9c display the peak-to-peak line width data in the ac, bc and ab planes, respectively and, as predicted by Eq. (9), it is observed that the shape of the observed angular variations of the width follows the angular dependences drawn in Figs. 7b, 8b and 9b. In the case of the ab plane, this happens only in the narrow angular ranges around the axes, where one line is observed. The lines in Figs. 7c, 8c and 9c

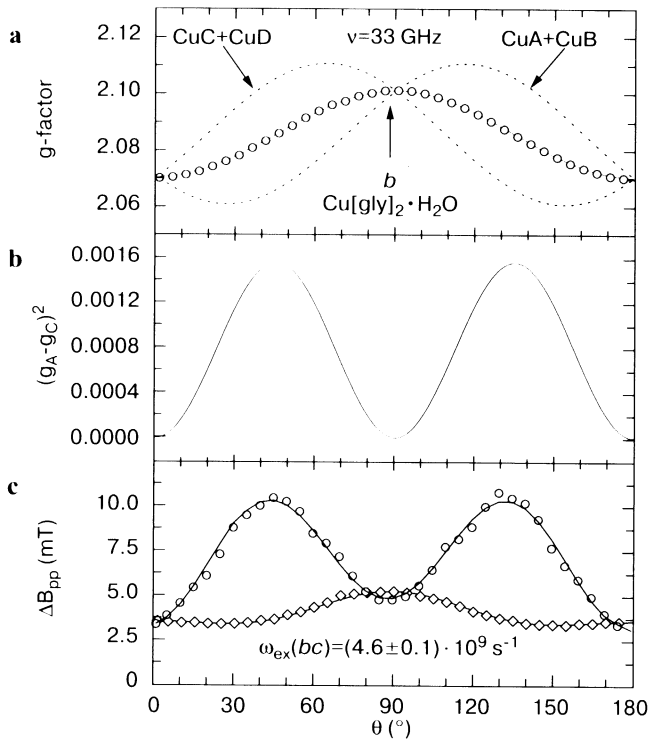

Fig. 8. **a** g-values of the resonance line observed for B_0 in the bc plane (circles) [28]. The dotted lines display the angular variation calculated for the molecular g-values. **b** Square of the difference between the molecular g-values plotted in **a**. **c** Peak-to-peak line width observed at 9.7 (◇) and 33 (○) GHz in the bc plane. The solid lines were obtained by fitting Eq. (9) to the data [28].

are obtained from fits of Eq. (9) to the data that allowed evaluating the exchange frequencies $\omega_{ex}(ac)$, $\omega_{ex}(bc)$ and $\omega_{ex}(ab)$ associated to these planes. As explained in ref. 28, these fits also consider contributions from dipolar interactions, which are not analyzed here.

Another piece of information about $[Cu(gly)_2]\cdot H_2O$ is provided by Fig. 3. The collapse of the lines in the ab plane is produced when their Zeeman energies in angular frequency units are equal to the exchange frequency $\omega_{ex}(ab)$ ($x = 1$). Martino et al. [28] discuss other possibilities of calculating $\omega_{ex}(ab)$ and show that all of them give the same results within the experimental uncertainties. The values obtained from the data at 33 GHz in the three crystal planes are

$$\omega_{ex}(ab) = (2.5 \pm 0.4)\cdot 10^9 \text{ 1/s},$$
$$\omega_{ex}(bc) = (4.6 \pm 0.1)\cdot 10^9 \text{ 1/s},$$
$$\omega_{ex}(ac) = (7.6 \pm 0.1)\cdot 10^9 \text{ 1/s},$$

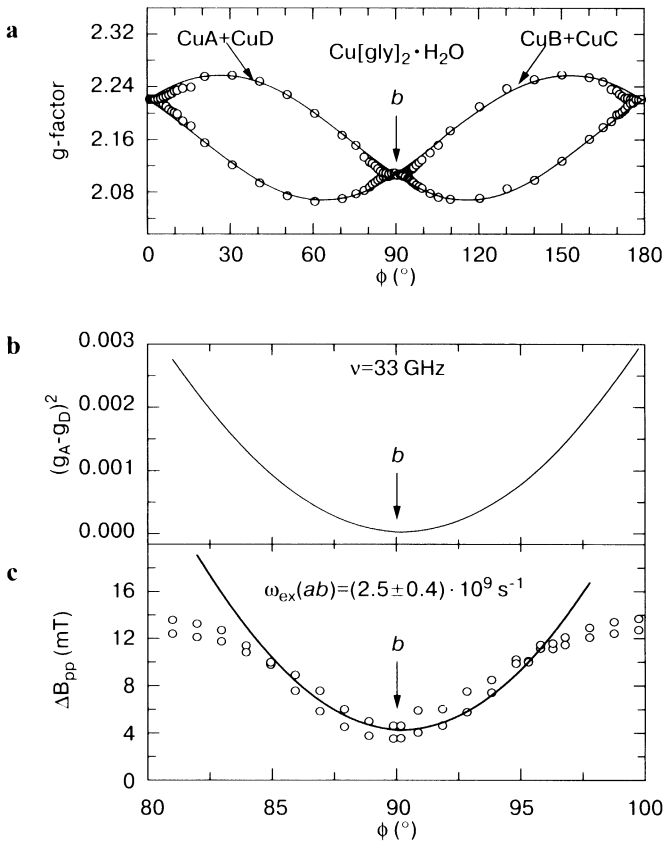

Fig. 9. **a** g-values of the resonance lines observed [28] for B_0 in the ab plane (circles). The dotted lines display the angular variation calculated for the molecular g-values. **b** Square of the difference between the molecular g-values plotted in **a**. **c** Peak-to-peak line width observed at 33 GHz in the ab plane (circles). The solid lines were obtained by fitting Eq. (9) to the data [28]. Plots **b** and **c** are drawn in the narrow collapsed resonance regime around the b axis.

that have the same order of magnitude. As shown by Figs. 7b, c, 8b, c, and 9b, c, the different behavior of the spectra in the three planes is not only a consequence of different values of ω_{ex}, but also a consequence of the differences in the molecular g-factors in the three crystal planes (Figs. 7b, 8b, and 9b).

The relations between the exchange frequencies $\omega_{ex}(ab)$, $\omega_{ex}(bc)$ and $\omega_{ex}(ac)$ and the exchange parameters obtained using Eq. (10), considering the structural information discussed above (Fig. 5), are

$$[\omega_{ex}(ab)]^2 = [2(J_{AB_1})^2 + 2(J_{AB_2})^2 + 2(J_{AC})^2]^2/\hbar^2, \tag{11a}$$

$$[\omega_{ex}(ac)]^2 = [2(J_{AC})^2 + 2(J_{AD})^2]^2/\hbar^2, \tag{11b}$$

$$|\omega_{ex}(bc)|^2 = |2(J_{AB_1})^2 + 2(J_{AB_2})^2 + 2(J_{AD})^2|^2/\hbar^2. \quad (11c)$$

The experimental results show qualitatively that $\omega_{ex}(ab)$ is small, and so should be J_{AB_1}, J_{AB_2} and J_{AC} (see Eq. (11a)). Thus, considering Eqs. (11b, c), the coupling J_{AD} should be the main responsible of $\omega_{ex}(ac)$ and $\omega_{ex}(bc)$. According to Martino et al. [28], this leads to a system where from the point of view of the EPR spectrum CuA and CuD (and CuB and CuC) form coupled spin subsets which give rise to each of the resonances observed in the *ab* plane. By Eqs. (11) the value $|J_1| = 0.028$ cm^{-1} can be estimated for the intrasubset exchange coupling. Also, using the value of $\omega_{ex}(ab)$ one can estimate $|J_2| = 0.009$ cm^{-1} for the intersubset exchange coupling (factors $2^{1/2}$ arising from the values of Z in Eq. (10) are missing in ref. 28). If one tries to calculate $J_{AB} = ((J_{AB_1})^2 + (J_{AB_2}))^{1/2}$, J_{AC} and J_{AD} from the experimental values of ω_{ex} by solving the system of Eqs. (11), it is observed that no real set of values is obtained. We attribute this problem to the validity of Eqs. (9) and (10) when the exchange couplings have the same order of magnitude. In that case one should consider nonsecular and higher-order corrections when obtaining Eq. (10) from a quantum model using the Kubo and Tomita theory. For cases where the differences in the magnitudes of the coupling are large [39, 40, 52–54], this problem does not occur. More theoretical work is being done in this direction to solve the problem.

4.3 Magneto-structural Correlations

The experimental result assigns the largest coupling $|J_{AD}| \approx |J_1| = 0.028$ cm^{-1} to the chemical path CuA–O-5–H$\cdots$O-2–C-2–O-1–CuC (Fig. 5d), This path contains a relatively strong noncovalent bond of the Cu ion with the water oxygen O-5 at the apical position, a strong H bond between O-5 and the carboxylate oxygen O-2 and the strong carboxylate bond O-2–C-2–O-1 equatorially connected to the other Cu ion and a CuA ion is connected to two CuD ions by bridges like this. This bridge contains 5 diamagnetic atoms, connects Cu ions at 0.7652 nm, and the length measured along the bond is 0.962 nm. Even if the complete magnetic network of $[Cu(gly)_2]\cdot H_2O$ cannot be solved, as explained above, the experimental information available seems to be clear about this assignment. It indicates that the equatorial-apical carboxylate bridge (Fig. 5a) is a weak magnetic connection between coppers (CuA and CuC in this case). This could be explained by the fact that the apical bond Cu–O-2 is long and consequently weak ($d = 0.2656$ nm), and as found for other cases [46], this bond segment is the main responsible for the strength of the coupling (see also [51]).

The intersubset coupling $|J_2| = 0.009$ cm^{-1} evaluated by Martino et al. is more difficult to assign and probably both $(J_{AB_1})^2 + (J_{AB_2})^2$ and $(J_{AC})^2$ contribute to the value of $\omega_{ex}^2(ab)$ in Eq. (11a). As explained above, more theoretical work following the procedures of ref. 40 and the theory of Kubo and Tomita [27] has to be done in this direction.

5 Selected Experimental Results

We discuss here values of the exchange couplings transmitted through three types of chemical bonds, equatorial-apical carboxylate bridges (a short bridge with three diamagnetic atoms) and longer bridges including H bonds and π-cation contacts. They were evaluated by the EPR techniques described above and are compared with experimental results obtained by thermodynamic techniques.

5.1 Equatorial-Apical Carboxylate Bridges

The type of superexchange pathway CuA–O_{eq}–C–O_{ap} · · · CuB, described in the inset of Fig. 10, includes three diamagnetic atoms, distances $d' \sim 0.52$ nm between Cu ions and $d' \sim 0.71$ nm when they are measured along the bond. It has been observed in several copper-amino acid and copper-peptide compounds and the values of the exchange coupling $|J|$ calculated from EPR line width data at 9 and 35 GHz in three similar compounds ($Cu(L\text{–}Phe)_2$, $Cu(L\text{–}Leu)_2$, $Cu(L\text{–}Met)_2$ [38, 43, 44], in which the Cu ions are connected by this bridge are plotted in Fig. 10 as a function of the distance between the Cu ion and the apical ligand (the weakest segment of the bridge indicated with a dashed line in Fig. 10, inset). In these cases the dihedral angles between the carboxylate bridge and the equatorial planes of the two copper ions are similar [51]. They display a clear linear dependence that was interpreted [46] considering that this segment of the exchange path was the limiting factor in the magnitude of the exchange when compared with the other covalent segments. Recent magnetic susceptibil-

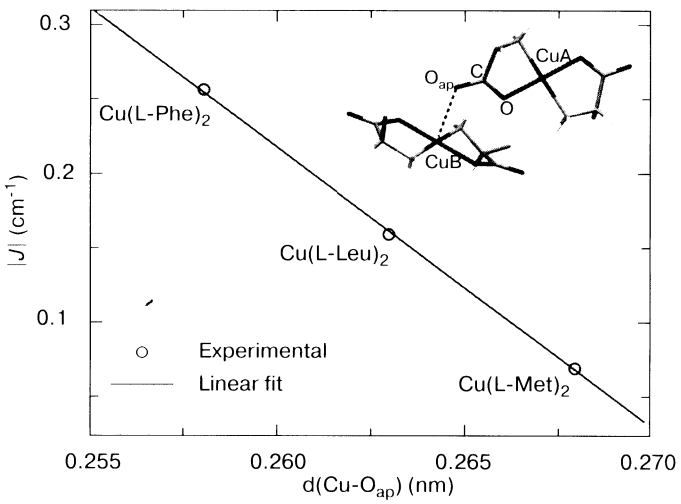

Fig. 10. Dependence of the exchange coupling with the distance of a Cu ion to the apical oxygen bond in compounds with similar equatorial-apical carboxylate pathways.

ity measurements in $Cu(L\text{-}Arg)_2 \cdot NO_3$ (C. Aiassa et al., Universidad Nacional del Litoral, Santa Fe, Argentina, pers. commun.), also showing a similar equatorial-apical carboxylate bridge as the superexchange pathway between Cu ions, indicated that the interaction is antiferromagnetic and its magnitude follows the behavior observed for the other compounds in Fig. 10. This result shows that EPR and magnetic measurements provide complementary data in order to analyze magneto-structural correlations.

5.2 Bridges Containing H Bonds

H bonds are important in most chemical pathways in proteins [62] and much effort has been directed to elucidate the role of these bonds in the transmission of exchange interactions.

We recently reported an extremely weak exchange coupling $|J| = 1.2 \cdot 10^{-3}$ cm^{-1} between Cu ions separated by a 1.317 nm thick layer of water molecules, in the copper compound of the peptide Ala-Phe [54]. The length of the pathway which contains 11 diamagnetic atoms including three H bonds is 1.834 nm. This interaction complements those transmitted through much stronger equatorial-equatorial carboxylate and amidato groups, which are estimated to be more than three orders of magnitude stronger and cannot be evaluated by EPR.

Another compound having H bonds studied recently is $Cu(II)(L\text{–arginine})_2 \times SO_4 \cdot (H_2O)_6$ [53]. The EPR results at 9.77 and 34.1 GHz in single-crystal samples of this ternary copper amino acid complex allowed to estimate exchange interactions $|J_1| = 0.6$ cm^{-1} and $|J_2| = 0.006$ cm^{-1} between copper neighbors at 0.5908 nm and at 1.5684 nm, respectively. J_1 is assigned to a syn-anti equatorial-apical carboxylate bridge with a total bond length of 0.7133 nm. J_2 is assigned to a long bridge of 12 atoms with a total bond length of 1.9789 nm that includes two hydrogen bonds. We showed that J_2 agrees with the exchange interaction observed between the reduced quinone acceptors $Q_A^{\bullet -}$ and $Q_B^{\bullet -}$ in the photosynthetic reaction center protein of the bacterium *Rhodobacter sphaeroides* [15, 16], which is transmitted along a similar chemical path containing two hydrogen bonds. These findings indicate that it is valid to estimate values for the exchange interactions between redox centers in proteins transmitted along long chemical paths containing sigma and H bonds, from data obtained in model systems, and emphasize the relevance of measuring exchange interactions in biologically relevant model systems.

Thermodynamic [63], EPR (N. M. C. Casado et al., Universidad Nacional del Litoral, Santa Fe, Argentina, unpubl.), and structural [64] measurements of the exchange coupling between Cu ions at 0.973 nm, connected by a chemical path containing 12 diamagnetic atoms including one H-bond were reported for the copper compound of the peptide Tyr-Leu. At temperatures above 1 K this compound displays specific heat and magnetic susceptibility characteristic of ferromagnetic spin chains with intrachain coupling $J = 2.50$ cm^{-1} [63]. At 0.16 K the magnetic properties show a discontinuity characteristic of a transition to a magneti-

cally ordered phase. The structure of Cu(II)Tyr-Leu displays copper ion chains with intrachain coupling supported by equatorial-equatorial syn-anti carboxylate bridges. In the perpendicular direction, Cu ions at $d = 0.973$ nm in neighbor chains are interconnected by paths containing 12 diamagnetic atoms including one H bond with a total bond length $d' = 1.912$ nm. These interchain connections and the associated exchange couplings are responsible of the transition to the magnetically ordered phase. A spin wave approximation allowed to estimate an interchain coupling $J' = 0.01$ cm $^{-1}$ from the transition temperature. EPR line width measurements in this system allowed to calculate $|J'| = 0.011$ cm^{-1} for the exchange interaction, in excellent agreement with the value obtained from the thermodynamic measurements. It is clear that the weakest segment in the interchain exchange path is the H-bond; the other segments are strong covalent bonds. The magnitude of the interchain exchange interaction is thus strongly dependent on the strength of this H bond.

5.3 Bridges Including π-Cation Contacts

Thermodynamic, EPR and structural measurements [50, 63, 65] have been reported for the copper complex of the peptide Trp-Gly. The structure of the compound displays spin chains with Cu ions connected by equatorial-equatorial syn-anti carboxylate bridges similar to those described for Cu(II)Tyr-Leu. Copper ions in neighbor chains at 1.05 nm chains are interconnected by two interchain pathways containing six and seven atoms, including a cation-π contact between a Cu ion and the indole ring of tryptophan. The specific heat and the susceptibility data above 1 K display a linear chain behavior with $J = 1.80$ cm^{-1} sustained by the carboxylate bridges. At 0.073 K, the specific heat and susceptibility data show a transition to a 3-D ordered magnetic phase [63]. Considering the temperature of the transition and using a spin wave model for the magnetic excitations it was estimated $J' = 0.051$ cm $^{-1}$ for the interchain interaction. This result is in good agreement with the value $|J'| = 0.042$ cm^{-1} obtained from EPR line width measurements [50] and shows that cation-π contacts are capable of transmitting exchange interactions. It also supports that the magnitudes of the exchange couplings provide a value characterizing the weakest chemical segments of the pathways.

6 Discussion

6.1 Comparison of EPR Results with Values Obtained from Nonresonance Techniques

Results of measurements of exchange interactions in model compounds performed using EPR were compared above with available values obtained in the same compounds by thermodynamic techniques (magnetization, susceptibility, and specific heat) with a good agreement considering the differences in the models used

to evaluate the interactions from each type of data. Other magnetic or specific heat measurements in copper complexes of amino acids and peptides have been reported by Newman et al. [66] for Cu(L-isoleucine)$_2$, by Calvo et al. [45] and Rapp et al. [67] for Cu(L-alanine)$_2$ and by Siqueira et al. [68] for Cu(L-but)$_2$ and Cu(D,L-but)$_2$ (but stands for 2-aminobutyric acid). In the analysis of the information it has to be considered that interactions connecting copper ions with identical positions in the lattice do not contribute to the EPR results. However, they may be the leading factors in the magnetic properties (see, for example, refs. 45, 47, 50, 55, 63, 67, 68). In other cases the thermodynamic measurements allow measuring interactions with magnitudes larger than those that can be observed by EPR [50, 63].

The agreement between the available values of the exchange interactions measured with the classical thermodynamic techniques and the results obtained from the EPR measurements supports the quality of the values obtained by EPR. This occurs for exchange couplings with magnitudes covering the range of interest for the purposes of this work.

6.2 Dependence of J on the Nature of the Unpaired Electrons for Long Chemical Pathways

The EPR measurements in model compounds described here have been performed in Cu(II) compounds. However, one wants to study chemical paths in proteins that connect other metal ions, radical ions, or metal ions with radical ions. The results presented in refs. 15, 16, 21, and 33 for the exchange couplings between different pairs of interacting metal ions and radicals in reaction centers of photosynthetic bacteria show that within less than one order of magnitude (which could be partially attributable to experimental uncertainty or to nonnegligible dipolar interactions) all results in this protein can be correlated with the same exponential dependence with distance. This result supports that when the chemical paths are long and weak, the main contribution to the magnitude of the exchange arises from the length of the path and the characteristics of their weak chemical segments, but not in the nature of the interacting unpaired electrons. Also, exchange interactions between radical ions in a protein [15, 16] and between copper ions in a model compound [53] that are connected by pathways containing similar segments have very similar magnitudes. With the information available at this moment one can assume that the magnitude of the exchange coupling depends mainly on the chemical pathways connecting the unpaired spins. The nature of these spins is less important for long pathways.

6.3 Magneto-structural Analysis

In a recent study [54] a procedure that may allow obtaining empirical rules to predict the magnitudes of exchange interactions transmitted along weak and long chemical bridges was proposed. The magnitude of the exchange interaction J

supported by a bridge containing p segments (σ-bonds or other noncovalent contacts) would be given by the function

$$J = J_0 \exp\left(\sum_{i=1}^{p} \eta_i\right), \tag{12}$$

where J_0 can be estimated from experimental information and η_i is a positive number which is small for strong covalent bonds (thus producing a small reduction of J) and large for H bonds or other weak bonds in the path. When the bridging system supporting the exchange interaction includes many atoms (and many bonds), Eq. (12) simplifies and gives a distance dependence that averages the individual characteristics of each bond. In a general case, Eq. (12) would give a better description of the change of J with the detailed properties of the bond and may have a broader applicability when more experimental results become available. Similar distance dependences have been proposed for the matrix elements of electron transfer processes [69, 70], and in view of the correlation between the two types of phenomena, comparison of results obtained from both sources would be complementary.

To perform this task (Eq. (12)), two types of goals have to be completed. The first is experimental: more model systems covering different possibilities for these long bonds have to be studied. The second is theoretical: more work has to be done in order to obtain a better understanding of the relation between exchange frequencies (evaluated in the EPR experiments) and exchange couplings which are assigned to specific chemical bridges. Part of this plan is already being performed. More model compounds containing chemical paths including H bonds are being studied by EPR and characterized by the qualities of these bonds and by the magnitudes of the exchange (N. M. C. Casado et al., unpubl.). More theoretical work is also being performed.

6.4 Changes in Magnetic Dimension Detected by EPR

Magnetically low-dimensional systems result when there are large differences in the exchange couplings along different directions in a material. They are important for physicists and deserve special consideration [71]. The dynamic response of the spins displays diffusive properties, and thus it is strongly dependent on the magnetic dimensionality. During our investigations of model compounds we observed that compounds containing L and D,L racemic mixtures of the same amino acid (methionine and 2-amino butyric acid) have different magnetic dimensionalities [55]. The crystal structures of the L and D,L compounds are very similar. However, the copper ions occupy sites with inversion symmetry in the D,L compounds but they do not in the compounds containing the L-amino acid. In the L compounds the spin dynamics tends to be 1-D, whereas the spin dynamics of the D,L compounds tends to be $2\frac{1}{2}$D, and this is detected in the EPR

experiments (see ref. 55 for details). The type of measurements discussed in this work can provide useful information in this direction.

6.5 Analyzing Experiments Using Generalized Bloch Equations

It has been mentioned before that the type of experiments that are presented here can be analyzed using the generalized Bloch equations method [20, 25, 29, 34, 35, 72]. In fact, when experimental data taken in the same conditions were compared [28, 29], the results were compatible. The problem observed using Bloch's equations is that the last stage of the problem, i.e., calculating values for the exchange interaction parameters from the data, cannot be clearly completed because the approach is essentially classical and there is not an analysis of the spectrum in terms of the spin Hamiltonian parameters. That is provided by the quantum theory of Kubo and Tomita [27], which allows performing the interface between the experimental results and the fundamental problem.

7 Conclusions

This work reviews methods to evaluate weak exchange couplings between metal ions in model compounds containing chemical paths similar to those encountered in biological molecules. Our purpose is to show the usefulness of these types of measurements to characterize chemical pathways that are important for the structure and function of proteins. The ideas of narrowing and collapse of magnetic resonance lines as a consequence of the exchange interactions between the unpaired spins introduced by Anderson [26] and Kubo and Tomita [27] are described and applied to the EPR measurements. We studied single-crystal samples of the model compounds and evaluated weak exchange couplings, 10^{-3} cm$^{-1} < J < 1$ cm^{-1}, a range of values which has received limited attention before. The described EPR measurements of the couplings are simpler than those performed with thermodynamic techniques, which require in general sophisticated equipment working below 1 K. Also, the calculation of the exchange parameters from the data is direct, requiring in most cases a simpler modeling of the systems than the thermodynamic measurements. These measurements also allow measuring simultaneously couplings with magnitudes differing by as much as three orders of magnitude.

It is not possible at this moment to review in a unified presentation all the data reported in the literature, which have been obtained and defined in different ways. However, we describe a selected group of results and discuss qualitatively the magneto-structural correlations emerging from the comparison of magnetic and structural data. The roles of molecular segments characteristic of proteins (weak carboxylate bridges, H bonds and cation-π interactions) in the transmission of exchange couplings are discussed. Also, the EPR results are compared with values obtained in some systems using thermodynamic techniques. The ad-

equacy of the studied compounds as model systems for weak exchange interactions in proteins is analyzed. I discuss problems pending to be solved and give my points of view of the future of this line of research

Acknowledgments

This paper is dedicated to George Feher, a great scientist, teacher and friend, in celebration of his 80th birthday (2004) and of the 50 years anniversary of his discovery of ENDOR (2006). Special thanks to Mario C. G. Passeggi for many years of illuminating discussions. The labeling of the atoms and the unit cell definition for $Cu[gly]_2H_2O$ were chosen as in Freeman et al. [59]. I am grateful to Ricardo Baggio for transforming the results reported in ref. 61 to this definition. I am very grateful to all the collaborators, colleagues and students with whom many experiments whose results are reviewed in this paper were performed, discussed and interpreted. I thank the Spanish Research Council (CSIC) for providing a free-of-charge license to the Cambridge Structural Database [73, 74]. This research project is supported by grants CAI+D-UNL 19-129 (2002), PIP 5274 and ANPCyT PICT 06-13782. I am a member of CONICET.

References

1. Kahn O.: Molecular Magnetism. New York: VCH 1993.
2. Slichter C.: Principles of Magnetic Resonance, 3rd edn. New York: Springer 1996.
3. Anderson P.W.: Phys. Rev. **115**, 2–13 (1959)
4. Hay P.J., Thibeault J.C., Hoffmann R.: J. Am. Chem. Soc. **97**, 4884–4899 (1975)
5. Kahn O.: Angew. Chem. Int. Ed. Eng. **24**, 834–850 (1985)
6. O'Connor C.J.: Prog. Inorg. Chem. **29**, 203–283 (1982)
7. Carlin R.L.: Magnetochemistry. Berlin: Springer 1986.
8. Bleaney B., Bowers K.D.: Proc. R. Soc. Lond. A **214**, 451–465 (1952)
9. Bencini A., Gatteschi D.: Electron Paramagnetic Resonance of Exchange Coupled Systems. Berlin: Springer 1994.
10. Perutz M.F.: Philos. Trans. R. Soc. A **345**, 105–112 (1993)
11. Lippard S.J., Berg J.M.: Principles of Bioinorganic Chemistry. Mill Valley, Calif.: University Science Books 1994.
12. Okamura M.Y., Isaacson R.A., Feher G.: Biochim. Biophys. Acta **546**, 394–417 (1979); Okamura M.Y., Fredkin D.R., Isaacson R.A., Feher G. in: Tunneling in Biological Systems (Chance B., DeVault D.C., Frauenfelder H., Marcus R.A., Suttin N., eds.), pp. 729–743. New York: Academic Press 1979.
13. De Vault D.C. in: Quantum Mechanical Tunneling in Biological Systems, pp. 118–121. London: Cambridge University Press 1984.
14. Bominaar E.L., Achim C., Borshch S.A., Girerd J.J., Münck E.: Inorg. Chem. **36**, 3689–3701 (1997)
15. Calvo R., Abresch E.C., Bittl R., Feher G., Hofbauer W., Isaacson R.A., Lubitz W., Okamura M.Y., Paddock M.L.: J. Am. Chem. Soc. **122**, 7327–7341 (2000)
16. Calvo R., Isaacson R.A., Paddock M.L., Abresch E.C., Okamura M.Y., Maniero A-L., Brunel L-C., Feher G.: J. Phys. Chem. B **105**, 4053–4057 (2001)
17. Chen P., Solomon E.I.: Proc. Natl. Acad. Sci. USA **101**, 13105–13110 (2004)
18. Weiss E.A., Wasielewski M.R., Ratner M.A.: J. Chem. Phys. **123**, 064504 (2005)

19. Coffman R.E., Buettner G.R.: J. Phys. Chem. **83**, 2387–2392 (1979)
20. Hoffmann S.K., Hilczer W., Goslar J.: Appl. Magn. Reson. **7**, 289–321 (1994)
21. Calvo R., Isaacson R.A., Abresch E.C., Okamura M.Y., Feher G.: Biophys. J. **83**, 2440–2456 (2002)
22. Butler W.F., Johnston D.C., Shore H.B., Fredkin D.R., Okamura M.Y., Feher G: Biophys. J. **32**, 967–992 (1980)
23. Abragam A., Bleaney B.: Electron Paramagnetic Resonance of Transition Ions. Oxford: Clarendon Press 1970.
24. Pilbrow J.R.: Transition Ion Electron Paramagnetic Resonance. Oxford: Clarendon Press 1990.
25. Weil J.A., Bolton J.R., Wertz J.E.: Electron Paramagnetic Resonance. Elementary Theory and Practical Applications, chapt. 10. New York: Wiley 1994.
26. Anderson P.W., Weiss P.R.: Rev. Mod. Phys. **25**, 269–276 (1953); Anderson P.W.: J. Phys. Soc. Jpn. **9**, 316–339 (1954); Abragam A.: The Principles of Nuclear Magnetism, chapt. X. London: Oxford University Press 1961.
27. Kubo R., Tomita K.: J. Phys. Soc. Jpn. **9**, 888–919 (1954)
28. Martino D.M., Passeggi M.C.G., Calvo R., Nascimento O.R.: Physica B **226**, 63–75 (1996)
29. Hoffmann S.K., Goslar J., Szczepaniak L.S.: Phys. Rev. B **37**, 7331–7337 (1988)
30. Poole C.P., Farach H.A.: The Theory of Magnetic Resonance, chapt. 3. New York: Wiley-Interscience 1972.
31. Bleaney B., Bowers K.D.: Proc. R. Soc. Lond. A **214**, 451–465 (1952)
32. Stoll S., Schweiger A.: J. Magn. Reson. **178**, 42–55 (2006). EasySpin is available at http://www.easyspin.ethz.ch/
33. Calvo R., Passeggi M.C.G., Isaacson R.A., Okamura M.Y., Feher G.: Biophys. J. **58**, 149–165 (1990)
34. Hoffmann S.K.: Chem. Phys. Lett. **98**, 329–333 (1983)
35. Hilczer W., Hoffmann S.K.: Chem. Phys. Lett. **144**, 199–203 (1988)
36. Pake G.E.: Paramagnetic Resonance. New York: Benjamin 1962.
37. Yokota M., Koide S.: J. Phys. Soc. Jpn. **9**, 953–960 (1954)
38. Levstein P.R., Steren C.A., Gennaro A.M., Calvo R.: Chem. Phys. **120**, 449–459 (1988)
39. Brondino C.D., Casado N.M.C., Passeggi M.C.G., Calvo R.: Inorg. Chem. **32**, 2078–2084 (1993)
40. Passeggi M.C.G., Calvo R.: J. Magn. Reson. A **114**, 1–11 (1995)
41. Van Kampen N.G.: Stochastic Processes in Physics and Chemistry. Amsterdam: North-Holland 1981.
42. Martino D.M., Passeggi M.C.G., Calvo R.: Phys. Rev. B **52**, 9466–9476 (1995)
43. Gennaro A.M., Levstein P.R., Steren C.A., Calvo R.: Chem. Phys. **111**, 431–438 (1987)
44. Steren C.A., Gennaro A.M., Levstein P.R., Calvo R.: J. Phys.: Condens. Matter **1**, 637–642 (1989)
45. Levstein P.R., Calvo R., Castellano E.E., Piro O.E., Rivero B.E.: Inorg. Chem. **29**, 3918–3922 (1990)
46. Levstein P.R., Calvo R.: Inorg. Chem. **29**, 1581–1583 (1990)
47. Calvo R., Passeggi M.C.G., Novak M.A., Symko O.G., Oseroff S.B., Nascimento O.R., Terrile M.C.: Phys. Rev. B **43**, 1074–1083 (1991)
48. Sartoris R.P., Ortigoza L., Casado N.M.C., Calvo R., Castellano E.E., Piro O.E.: Inorg. Chem. **38**, 3598–3604 (1999)
49. Costa-Filho A.J., Munte C.E., Barberato C., Castellano E.E., Mattioli M.P.D., Calvo R., Nascimento O.R.: Inorg. Chem. **38**, 4413–4421 (1999)
50. Costa-Filho A.J., Nascimento O.R., Ghivelder L., Calvo R.: J. Phys. Chem. B **105**, 5039–5047 (2001)
51. Schveigkardt J.M., Rizzi A.C., Piro O.E., Castellano E.E., Santana R.C., Calvo R., Brondino C.D.: Eur. J. Inorg. Chem. **2002**, 2913–2919.
52. Costa-Filho A.J., Nascimento O.R., Calvo R.: J. Phys. Chem. B **108**, 9549–9555 (2004)
53. Santana R.C., Cunha R.O., Carvalho J.F., Vencatto I., Calvo R.: J. Inorg. Biochem. **99**, 415–423 (2005)
54. Vieira E.D., Casado N.M.C., Facchin G., Torre M.H., Costa-Filho A.J., Calvo R.: Inorg. Chem. **45**, 2942–2947 (2006)
55. Levstein P.R., Pastawski H.M., Calvo R.: J. Phys.: Condens. Matter **3**, 1877–1888 (1991)
56. Abe H., Ono K.: J. Phys. Soc. Jpn. **11**, 947–956 (1956)

57. Calvo R., Mesa M.A.: Phys. Rev. B **28**, 1244–1248 (1983)
58. Tomita K., Nitta I.: Bull. Chem. Soc. Jpn. **34**, 286–291 (1961)
59. Freeman H.C., Snow M.R., Nitta I., Tomita K.: Acta Crystallogr. **17**, 1463–1470 (1964)
60. Moussa S.M., Fenton R.R., Hunter B.A., Kennedy B.J.: Austr. J. Chem. **55**, 331–341 (2002)
61. Casari B.M., Mahmoudkhani A.H., Langer V.: Acta Crystallogr. E **60**, m1949–m1951 (2004)
62. Jeffrey G.A.: An Introduction to Hydrogen Bonding. New York: Oxford University Press 1997.
63. Chagas E.F., Rapp R.E., Rodrigues D.E., Casado N.M.C., Calvo R.: J. Phys. Chem. B **110**, 8052–8063 (2006)
64. Baggio R., Casado N.M.C., Calvo R., Rapp R.E., Garland M.T.: Acta Crystallogr. C **61**, m250–m252 (2005)
65. Nascimento O.R., Costa A.J., De Morais D.I., Ellena J., Delboni L. F.: Inorg. Chim. Acta **312**, 133–138 (2001)
66. Newman P.R., Imes J.L., Cowen J.A.: Phys. Rev. B **13**, 4093–4097 (1976)
67. Rapp R.E., de Souza E.P., Godfrin H., Calvo R.: J. Phys.: Condens. Matter **7**, 9595–9606 (1995)
68. Siqueira M.L., Rapp R.E., Calvo R.: Phys. Rev. B **48**, 3257–3263 (1993)
69. Beratan D.N., Onuchic J.N., Hopfield J.J.: J. Chem. Phys. **86**, 4488–4498 (1987)
70. Onuchic J.N., Beratan D.N.: J. Chem. Phys. **92**, 722–733 (1987)
71. Dietz R.E., Merrit F.R., Dingle R., Hone D., Silbernagel B.G., Richards P.M.: Phys. Rev. Lett. **26**, 1186–1188 (1971); Richards P.M., Salamon M.B.: Phys. Rev. B **9**, 32–45 (1974); Richards P.M. in: Local Properties at Phase Transitions, pp. 539–570. Bologna: Editrice Compositori 1975.
72. Karunakaran C., Thomas K.R.J., Shunmugasundaram A., Murugesan R.: Mol. Phys. **100**, 287–295 (2002)
73. Allen F.H.: Acta Crystallogr. B **58**, 380–388 (2002)
74. Bruno I.J., Cole J.C., Edington P.R., Kessler M., Macrae C.F., McCabe P., Pearson J., Taylor R.: Acta Crystallogr. B **58**, 389–397 (2002)

Author's address: Rafael Calvo, Departamento de Física, Facultad de Bioquímica y Ciencias Biológicas, Universidad Nacional del Litoral, Güemes 3450, 3000 Santa Fe, Argentina